IEEE Sensors Journal

4.5 Impact Factor	**0.06589** Eigenfactor
0.746 Article Influence Score	**8.2** CiteScore Powered by Scopus

Home | Popular | Early Access | Current Issue | All Issues | About Journal

Submit Manuscript
Submission Guidelines
Become a Reviewer
Open Access Publishing Options
Add Title To My Alerts
Add to My Favorites

Aims & Scope

According to the IEEE Sensors Council's constitution, "The fields of interest of the Council and its activities shall be the theory, design, fabrication, manufacturing and application of devices for sensing and transducing physical, chemical, and biological phenomena, with emphasis on the electronics and physics aspects of sensors and integrated sensor-actuators." The *IEEE Sensors Journal* focuses on the numerous sensor technologies spanned by the IEEE, and on emerging sensor technologies.

Publication Fees

This publication is hybrid, meaning that it is supported by subscriptions and applicable article processing charges (APCs). Although there is no cost for publishing with IEEE, authors may wish to take advantage of some of our fee-based offerings, for example, choosing to publish open access in a hybrid journal. Visit the IEEE Author Center for more information on available options. The open access APC for this title is **$2,800 USD**. Learn more

Contact Information

Editor-in-Chief

Zeynep Celik
University of Texas at Arlington
Arlington
USA
zcelik@uta.edu

Editorial Board

Author Center

IEEE Sensors Journal

Popular | Recent | Most Cited

Information for Authors

Publishing Policies

A Lightweight Perception Enhancement Network For Real-Time And Accurate Internal Surface Defect Detection Of Cold-Drawn Steel Pipes

You Tan; Kechen Song; Hongshu Chen; Yu Zhang; Yunhui Yan

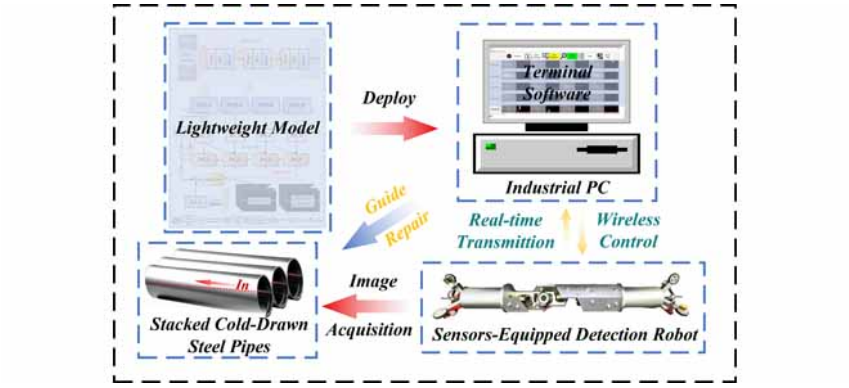

Smart Insoles With Textile Capacitive Sensors For Efficient Gait Phase Recognition

Panagiotis Mavrogiannis; Ilias Maglogiannis; Lazar Milić; Christos Panagopoulos; Andreas Menychtas; Goran M. Stojanović

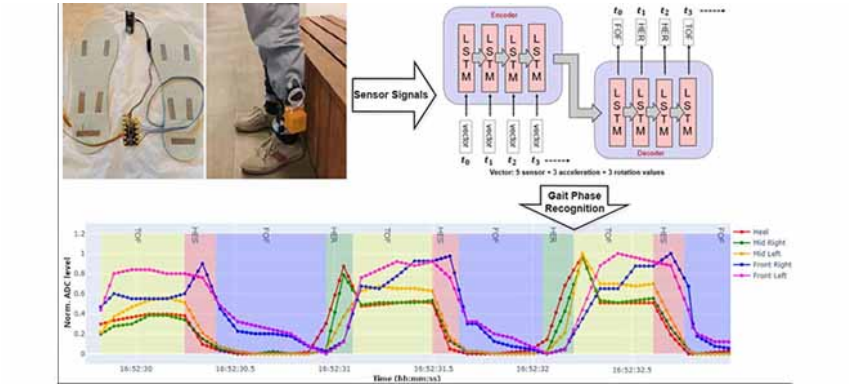

Unified Neural Network-Based Shape Sensing For Continuum Robots Using Fiber Bragg Gratings

Samuel Wild; Belal A. Elsayed; Hongshen Shi; Simon D. Jones; Tianyi Zeng; Abdelkhalick Mohammad; Dragos Axinte; Xin Dong

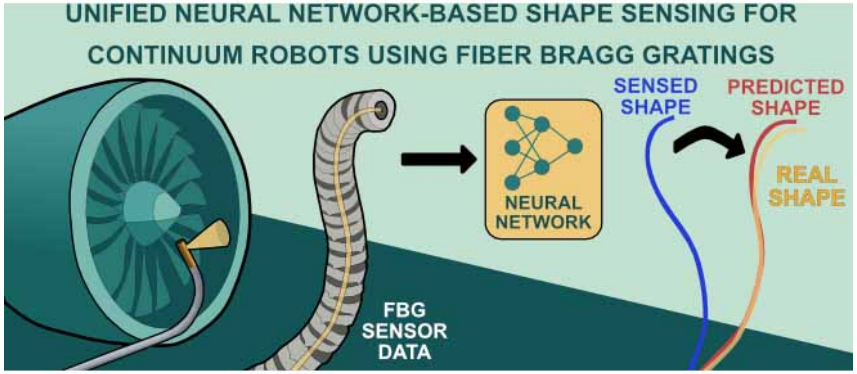

Silicon–Platinum Bowtie-Coupled Thermoelectric Terahertz Detector

Francisco Javier González; Robert E. Peale; Juan R. Moreno

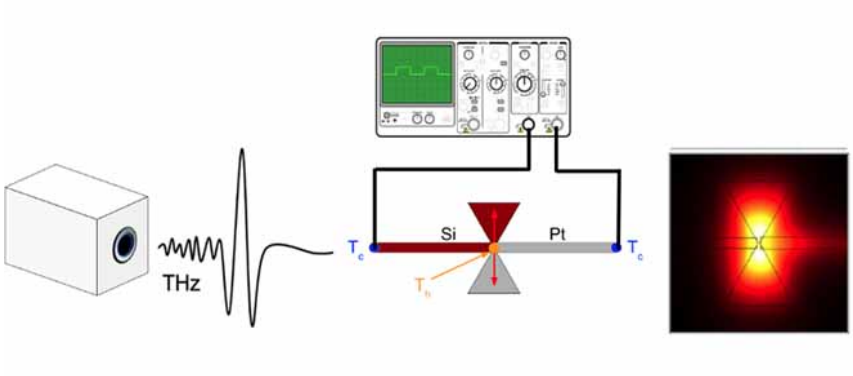

3D-Printed Airflow Hair Sensor Inspired By The Buthus Occitanus Scorpion's Flat Trichobothria

Samuele Martinelli; Andrew Reid; James F. C. Windmill

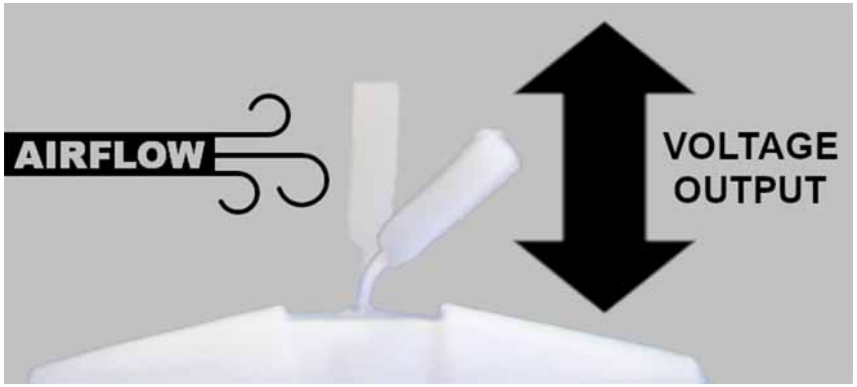

Show All

Related Magazines or Journals

IEEE Transacti
Components, Pa
and Manufac
Technolo

IEEE Access

IEEE Spectrum

IEEE Personal Account

CHANGE USERNAME/PASSWORD

Purchase Details

PAYMENT OPTIONS

VIEW PURCHASED DOCUMENTS

Profile Information

COMMUNICATIONS PREFERENCES

PROFESSION AND EDUCATION

TECHNICAL INTERESTS

Need Help?

US & CANADA: +1 800 678 4333

WORLDWIDE: +1 732 981 0060

CONTACT & SUPPORT

Follow

About IEEE *Xplore* | Contact Us | Help | Accessibility | Terms of Use | Nondiscrimination Policy | IEEE Ethics Reporting | Sitemap | IEEE Privacy Policy

A public charity, IEEE is the world's largest technical professional organization dedicated to advancing technology for the benefit of humanity.

Fabric-Based Metamaterial-Integrated CPW Antenna for Microwave Tumor Sensing

Publisher: IEEE

Cite This PDF

Intan Shafinaz Abd. Razak ; Ahmed Jamal Abdullah Al-Gburi ; Maizatul Alice Meor Said ; Syah Alam ; Zahriladha Zakaria **All Authors**

Abstract:
This study presents a fabric-based material that integrates a circular patch co-planar waveguide (CPW) antenna with a metamaterial (MTM), which is fabricated on a felt material for the purpose of microwave tumor sensing. The MTM comprises a 5 × 5 unit cell array of X-shaped MTM that works at 3.30–4.25 GHz to ensure the CPW antenna has better bandwidth and gain. The MTM-integrated antenna operates over a wide frequency range of 2.4–6.9 GHz, achieving a peak gain of 6.7 dBi and compact dimensions of 53 × 60 mm. Experiments were conducted using a rotating platform at 36◦ intervals to capture scattered data from a realized phantom representing a breast tumor model. The delay-and-sum (DAS) approach was employed to reconstruct a 2-D image from reflected and scattered signals obtained from ten different points around the phantom, both in the presence and absence of a 15-mm tumor. This wearable microwave imaging (MWI) device utilizes a single antenna and a monostatic radar-based approach. Correspondingly, the results indicate that integrating MTMs markedly enhances imaging precision by reducing the displacement of tumor images. The proposed design demonstrates promising results and is adaptable for tumor sensing. Additionally, the design exhibits potential for wearable applications, such as MWI and on-body communications.

Figures
References
Keywords
Metrics
More Like This

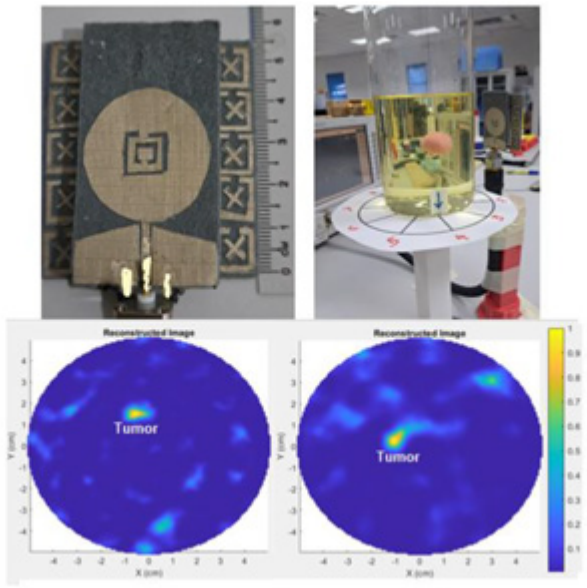

Published in: IEEE Sensors Journal (Volume: 26 , Issue: 3, 01 February 2026)

Page(s): 3944 - 3953

DOI: 10.1109/JSEN.2025.3642335

Date of Publication: 17 December 2025

Publisher: IEEE

ISSN Information:

Funding Agency:

I. Introduction

Breast cancer remains a major worldwide health issue, as evidenced by the 670 000 deaths recorded worldwide [1]. Therefore, regular screenings are crucial for the early detection of breast tumors. Traditional methods for breast imaging include ultrasound, mammography, and magnetic resonance imaging (MRI). However, the efficacy of ultrasonic imaging is heavily reliant on the proficiency of the performing physician [2]. Additionally, due to its low sensitivity, ultrasonic imaging is inappropriate for breasts with a high concentration of fat. MRI provides high

sensitivity, yet its primary disadvantage is its , many women perceive mammography as unpleasant and painful despite the health hazards associated with ionizing radiation. Notably, ionizing radiation renders many treatments unsuitable, particularly for younger women. Accordingly, microwave imaging (MWI) provides a nonionizing, cost-effective, and comfortable substitute for conventional techniques, such as mammography, MRI, and ultrasound [3], [4], [5]. With its ability to decrease radiation exposure, lower

Authors

Figures

References

Keywords

Metrics

Fabric-Based Metamaterial-Integrated CPW Antenna for Microwave Tumor Sensing

Intan Shafinaz Abd. Razak, Ahmed Jamal Abdullah Al-Gburi, *Senior Member, IEEE*, Maizatul Alice Meor Said, Syah Alam, *Member, IEEE*, and Zahriladha Zakaria, *Senior Member, IEEE*

***Abstract*—This study presents a fabric-based material that integrates a circular patch co-planar waveguide (CPW) antenna with a metamaterial (MTM), which is fabricated on a felt material for the purpose of microwave tumor sensing. The MTM comprises a 5 × 5 unit cell array of X-shaped MTM that works at 3.30–4.25 GHz to ensure the CPW antenna has better bandwidth and gain. The MTM-integrated antenna operates over a wide frequency range of 2.4–6.9 GHz, achieving a peak gain of 6.7 dBi and compact dimensions of 53 × 60 mm. Experiments were conducted using a rotating platform at 36° intervals to capture scattered data from a realized phantom representing a breast tumor model. The delay-and-sum (DAS) approach was employed to reconstruct a 2-D image from reflected and scattered signals obtained from ten different points around the phantom, both in the presence and absence of a 15-mm tumor. This wearable microwave imaging (MWI) device utilizes a single antenna and a monostatic radar-based approach. Correspondingly, the results indicate that integrating MTMs markedly enhances imaging precision by reducing the displacement of tumor images. The proposed design demonstrates promising results and is adaptable for tumor sensing. Additionally, the design exhibits potential for wearable applications, such as MWI and on-body communications.**

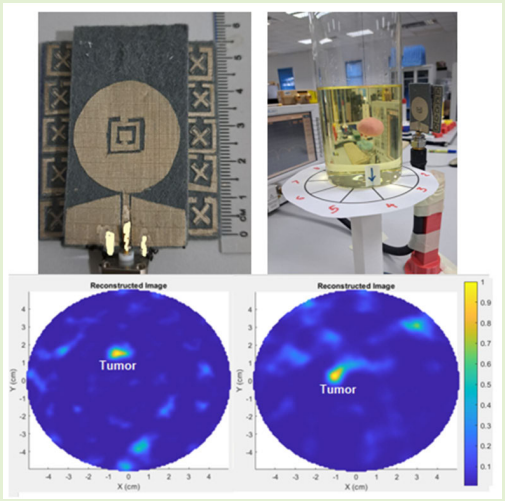

***Index Terms*—Co-planar waveguide (CPW) antenna, delay-and-sum (DAS) image algorithm, fabric-based antenna, metamaterial (MTM) antenna, monostatic radar-based approach, tumor sensing.**

I. Introduction

BREAST cancer remains a major worldwide health issue, as evidenced by the 670 000 deaths recorded worldwide [1]. Therefore, regular screenings are crucial for the early detection of breast tumors. Traditional methods for breast imaging include ultrasound, mammography, and magnetic resonance imaging (MRI). However, the efficacy of ultrasonic imaging is heavily reliant on the proficiency of the performing physician [2]. Additionally, due to its low sensitivity, ultrasonic imaging is inappropriate for breasts with a high concentration of fat. MRI provides high sensitivity, yet its primary disadvantage is its extensive expense. Furthermore, many women perceive mammography as unpleasant and painful despite the health hazards associated with ionizing radiation. Notably, ionizing radiation renders many treatments unsuitable, particularly for younger women. Accordingly, microwave imaging (MWI) provides a nonionizing, cost-effective, and comfortable substitute for conventional techniques, such as mammography, MRI, and ultrasound [3], [4], [5]. With its ability to decrease radiation exposure, lower implementation costs, and enhance patient comfort, this technology has significant potential as a tool for detecting early-stage cancer.

MWI is now being researched as an additional screening method for medical purposes, including breast cancer screening and brain diagnosis [6], [7]. Using the notable variation in dielectric characteristics between healthy and

Received 6 October 2025; revised 12 November 2025; accepted 25 November 2025. Date of publication 17 December 2025; date of current version 2 February 2026. This work was supported by the Universiti Teknikal Malaysia Melaka (UTeM) and Federal Training (HLP) Scholarship Schemes Awarded by Malaysian Ministry of Higher Education. The associate editor coordinating the review of this article and approving it for publication was Prof. Mohammad Hossein Zarifi. *(Corresponding author: Zahriladha Zakaria.)*

Intan Shafinaz Abd. Razak is with the Fakulti Teknologi dan Kejuruteraan Elektronik dan Komputer (FTKEK), Universiti Teknikal Malaysia Melaka (UTeM), Durian Tunggal 76100, Malaysia (e-mail: intanshafinaz81@gmail.com).

Ahmed Jamal Abdullah Al-Gburi, Maizatul Alice Meor Said, and Zahriladha Zakaria are with the Centre for Telecommunication Research and Innovation (CeTRI), Universiti Teknikal Malaysia Melaka (UTeM), Durian Tunggal 76100, Malaysia (e-mail: zahriladha@utem.edu.my).

Syah Alam is with the Department of Electrical Engineering, Universitas Trisakti, West Jakarta 11440, Indonesia.

Digital Object Identifier 10.1109/JSEN.2025.3642335

diseased tissues, the electromagnetic (EM) signal penetrates and absorbs the data used in certain algorithms to get image reconstruction. MWI typically employs radar-based systems that use bistatic, monostatic, or multistatic configurations for signal transmission and reception [8], [9]. However, the practical and widespread adoption of current MWI systems is impeded by two significant, often combined, limitations. The first factor is the physical form factor. Most antenna designs conventionally depend on rigid structures [10], [11], [12], [13], [14], [15], [16]. The preference for rigid antennas mainly stems from their stability, reliability, ease of manufacture, and repeatability, which have established them as the primary choice in MWI. Nevertheless, their rigidity makes them bulky and unsuitable for wearable applications. Several studies have employed flexible antennas for MWI, such as those in [17], [18], [19], [20], and [21]. Flexible antennas in MWI enable adaptable, patient-conforming designs, which are crucial for increasing comfort.

The second factor is the system complexity in terms of achieving sufficient imaging resolution; most high-performance systems [11], [13], [19], [20], [22] rely on complex, multiantenna arrays. This approach inherently increases system cost, physical bulk, and the computational complexity of the required image reconstruction algorithms. Meanwhile, studies in [17] and [18] exhibited favorable gain and utilized S-parameters to demonstrate tumor presence; however, there was no evidence for tumor image reconstruction. According to [21], a single antenna appears simple and promising, only operates in a very narrow bandwidth of 400 MHz, and has notably large dimensions (125 × 51 mm).

Concurrently, metamaterials (MTMs) have been studied by [10], [11], [12], [13], [14], [19], and [20] to improve antenna performance, increasing gain, directivity, and sensitivity are needed to detect the subtle dielectric contrast of small tumors. The use of MTM can produce a greater gain and expand the sensor's bandwidth. The high gain and broad operating bandwidth lead to high-resolution images and are used to capture signals that are reflected from tumors. The MTM flexible antenna array of [20] demonstrates that 12 antenna arrays yield a better tumor image compared to four and eight arrays. Note that 12 antenna arrays can mitigate skin layer clutter and artifacts solely through simulated findings. A flexible array by [19] incorporating a tumor model and image reconstruction has secured the previous MTM flexible antenna. Hence, adding four antennas enhanced image quality. Nevertheless, this design necessitated four RF varactor diodes, potentially complicating the circuitry.

A distinct research gap emerges at the intersection of these technologies. The literature shows that MTM enhancement is most often applied to complex, rigid arrays [13], [14] or complex flexible arrays [19], [20]. Conversely, simpler single-antenna (monostatic) systems, ideal for low-cost, simple setups, have been proposed in [15] and [16] but lack the conformal flexibility. Therefore, the main challenge is the absence of a straightforward, compact, and highly sensitive MWI system that combines all three essential components for a practical device: a single-element (monostatic) design, a conformal flexible substrate, and integrated MTM enhancement. This research aims to fill this gap by creating a monostatic, MTM-enhanced flexible antenna capable of biomedical imaging without the expense and complexity of a full array. To the best of our knowledge, there remains limited literature on fabric-based, inspired MTM integrated antennas in single sensors using a monostatic tumor detection approach in MWI.

Development using a split-ring resonator (SRR) is widely used in various sensing applications [23], [24], [25]. Notably, the unit cell is designed to integrate with the antenna, achieving resonance between 3 and 6 GHz for MWI purposes. The proposed CPW with MTM (CPWMTM) antenna covers a bandwidth of 2.4–6.9 GHz in simulations and 1.6–5.9 GHz in experimental measurements with a breast phantom. Correspondingly, the CPWMTM antenna sensor was validated using a monostatic radar-based method. This method involves the transmitter and receiver operating from a single antenna. This setup allows the system to send out waves and then receive the reflected signals after they bounce off an object, which is useful for various applications, including target detection and imaging [26]. The variation in scattered data, processed with a delay-and-sum (DAS) imaging algorithm coded in MATLAB, generates an image of the tumor. Remarkably, the CPWMTM antenna sensor requires only ten distinct points in the azimuth plane around the tumor model. This demonstrates its potential to reduce image clutter and improve tumor localization accuracy compared to the co-planar waveguide (CPW) antenna.

This article is organized as follows. Section II includes the antenna geometry and design. Subsequently, Section III describes the antenna performance analysis. Then, Section IV reviews the module's imaging performance for the breast model. Lastly, Section V specifies the conclusion of the study.

II. Fabric-Based MTM Integrated Antenna

A. Antenna Design

The design initiates with the antenna section. Fig. 1 illustrates the suggested antenna design. The graphic displays the overall size of the antenna. The dimensions of the antenna are 34 × 58 × 2 mm. The feed and a circular patch resonator are fabricated on the felt substrate material. Using an Agilent 85070 E Dielectric Probe Kit, the substrate material exhibited a dielectric constant of 1.398 and a loss tangent of 0.024. The feed dimensions are calibrated to correspond with a typical 50-Ω feed line, which is a coaxial signal cable. The design was selected to facilitate broadband functionality. As the broadband response achieved high-resolution imaging [27], [28] and deeper penetration [2], [27], [29] for material classification in multilayered structures [27], [30]. In particular, including a CSRR in the middle of the circular resonator improved the antenna's reflection coefficient.

The radiator patch and ground plane conductive layers are constructed using a 0.17-mm-thick ShieldIT super fabric from less EMF with 0.05-Ω/sq sheet resistance. This fabric comprises ripstop and woven polyester and is treated with copper and nickel [31], [32]. It has a calculated conductivity of 1.18×10^5 S/m [32]. Fig. 1(a) shows the layout and dimensions of the wearable microstrip antenna, as viewed from the front perspective. Meanwhile, Fig. 1(b) illustrates the parameters of the CSRR. The circular diameter of the antenna is 31.6 mm,

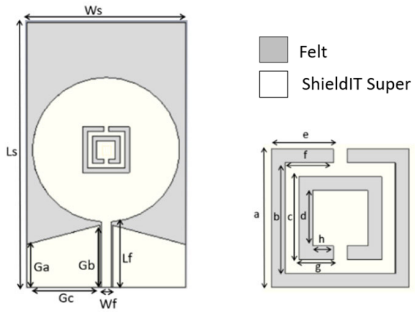

Fig. 1. CPW antenna (a) patch, feedline, and ground dimension, as well as (b) complementary SRR dimension.

TABLE I
GEOMETRIC PARAMETERS OF THE PROPOSED ANTENNA

Parameters	W_s	L_s	G_a	G_b	G_c
Values (mm)	34	58	9.42	13.6	15.6
Parameters	W_f	L_f	a	b	c
Values (mm)	2	14.33	10	8	6
Parameters	d	e	f	g	h
Values (mm)	4	4.5	3.5	2.5	1.5

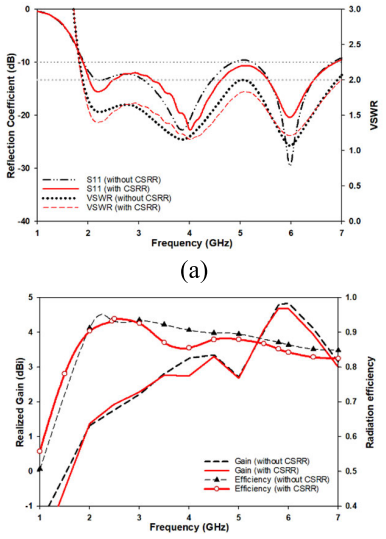

Fig. 2. Circular patch CPW simulation results reveal (a) reflection coefficient and VSWR and (b) gain and radiation efficiency.

and the other geometrical parameters of the antenna are represented in Fig. 1 and Table I. Meanwhile, the suitable dimensions are obtained by employing a parametric CST microwave analysis. In addition, the appropriate dimensions have been selected for the predetermined resonance frequency using the formula from [33].

Fig. 2(a) demonstrates that the CSRR reduces the reflection coefficient and increases impedance bandwidth and voltage standing wave ratio (VSWR). Fig. 2(b) illustrates the variation in antenna gain and radiation efficiency according to the design. The wideband antenna frequency range of 1.9–6.9 GHz indicates that the antenna operates effectively across the desired frequency band. This study employed a frequency range of 2–6 GHz to attain optimal penetration depth and high-resolution imaging for tumor detection, as supported by [5], [34], and [35]. Notably, the antenna's radiation efficiency exceeds 88%, with a realized gain between 1 and 4.7 dBi for the CPW structure with CSRR. A comparison of antenna characteristics is presented in Table II.

TABLE II
COMPARISON OF ANTENNA PARAMETERS

Characteristics	Without CSRR	With CSRR
Bandwidth (GHz)	1.9 to 4.8 and 5.2 to 6.8	1.9 to 6.9
Gain (dBi)	1.4 to 4.8	1.0 to 4.7
Radiation Efficiency (%)	85 to 93	88 to 94

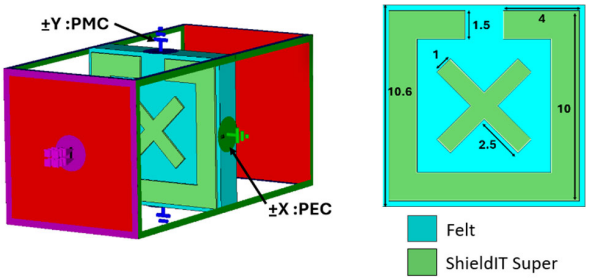

Fig. 3. Simulation of the boundary setup of the proposed unit cell.

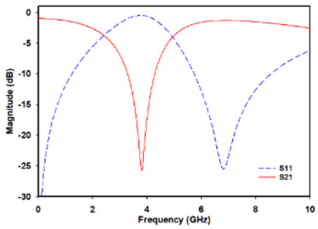

Fig. 4. Magnitude of the S-parameter (S_{11} and S_{21}) for the proposed unit cell.

B. Unit Cell Design and Integration

To obtain directive radiation patterns and increase gain and efficiency, MTM is widely used in numerous applications [36]. Each form of MTM has a distinct influence on the performance of an antenna concerning factors, such as gain, efficiency, polarization, and more, particularly when it is nearby as a ground plane, reflector, and superstrate [37], [38]. In this design, the MTM is located at the back of the CPW antenna. Hence, to derive accurate and relevant parameters, a high-frequency EM simulator called CST Microwave Studio (CST), based on the finite integration technique (FIT), was utilized.

The simulator functioned in the frequency range of 1–10 GHz with a hexahedral mesh setup. The study employed a transverse EM (TEM) wave traveling along the Z-axis to explain the interaction between the suggested MTM unit cell and array structure with the fields. Fig. 3 illustrates the application of perfect electric conductor (PEC) boundary conditions on the X-axis and perfect magnetic conductor (PMC) boundary conditions on the Y-axis [39].

Fig. 4 presents the S-parameters, which encompass both the reflection coefficient and the transmission coefficient. Observation has demonstrated that the transmission coefficient covers the frequency ranges of 3.30–4.25 GHz. The results obtained from CST are further supported by the Nicolson–Ross–Weir (NRW) method, as presented in [19], [39], and [40]. This

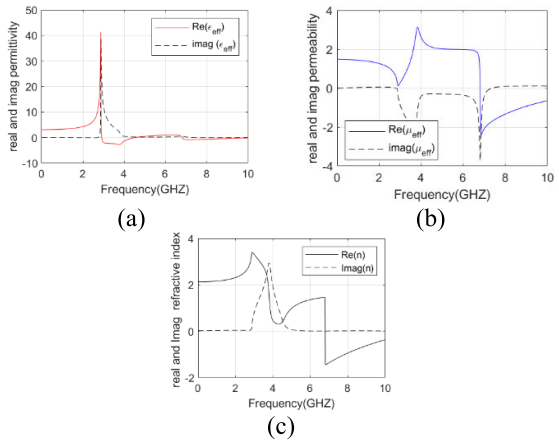

Fig. 5. Simulated results of the proposed unit cell (a) permittivity, (b) permeability, and (c) refractive index.

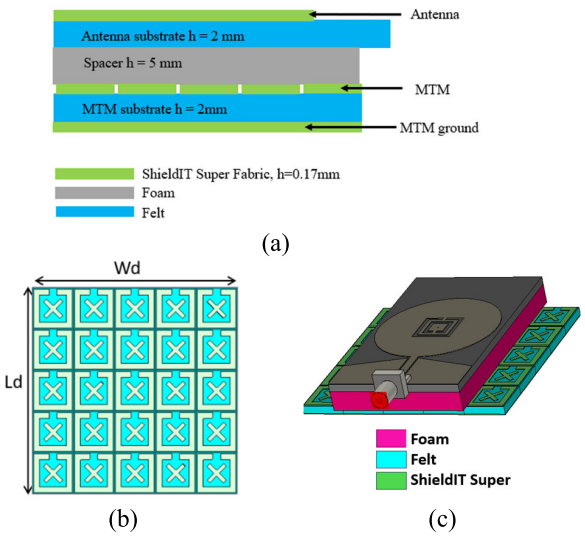

Fig. 6. CPW MTM antenna. (a) Cross section view of the antenna with the MTM, (b) proposed MTM array, and (c) cross section view of the antenna with the MTM array in CST simulation.

approach is essential for deriving necessary parameters, such as permittivity, permeability, refractive index, and impedance. The MATLAB simulation in Fig. 5 indicates the permeability, permittivity, and refractive index. Consequently, Fig. 5(a) indicates the frequency range encompassing the desired negative area. Specifically, the epsilon negative (ENG) emerges within the frequency zone of 2.9–4.3 GHz. It is observed that within the resonance frequencies covering from 3.30 to 4.25 GHz, the permittivity demonstrates negative values. This characteristic identifies the structure as a single negative (SNG) MTM. Consequently, the unit cell displays ENG properties, which are particularly noticeable with negative maximum permittivity near the resonance frequency of 3.77 GHz. The designed SNG MTM demonstrated an effective medium ratio (EMR) of 7.5, indicating a strong subwavelength characteristic. This high EMR value confirms the structure's suitability for low-frequency microwave applications, where compactness and enhanced EM response are essential [39]. The mu negative (MNG) is 6.8–10 GHz, as illustrated in Fig. 5(b).

The integration took place after optimizing the antenna and MTM construction. The primary focus in constructing the MTM structure is the reflection coefficient over the wideband operating frequency range. A 5-mm-thick layer of Rohacell foam material with 1.012 relative permittivity was inserted between the MTM and the antenna. The foam was used to function as a spacer, ensuring a fixed spacing and avoiding any electrical contact between the MTM and the antenna. Fig. 6(a) depicts the cross-sectional perspective of the antenna using the MTM. The cross-sectional view displays that the MTM structure comprises three layers: two metallic layers (MTM arrays and ground plane) and a dielectric substrate positioned between them.

The MTM cell size was optimized through simulations. The geometry of the suggested MTM structure is realized in Fig. 6(b). It is composed of a 5 × 5 square matrix, lined up with 25 square-shaped unit cells. With symmetrical spacing at each edge of the SRR, an X-shaped design is selected for the MTM, as its shape is uniform in all directions, and it also facilitates ease of production when implemented in measurement. Fig. 6(b) also displays that the MTM structure has the dimensions of 53 mm for width (W_d) and 53 mm for length (L_d) and that each MTM cell has the dimensions of 10 mm for side lengths (i.e., W_d and L_d with a 0.6-mm gap between each unit cell). The following investigation stage aims to determine the outcome of integrating the antenna and MTM. The experiment was conducted at the Microwave Laboratory, Universiti Teknikal Malaysia Melaka.

III. MTM-Integrated Antenna Performance Analysis

Following the antenna optimization, we developed an MTM structure and incorporated it into the rear to minimize the interference between the antenna and the human body. The primary concern in constructing the MTM structure is ensuring that the reflection coefficient, specifically the S_{11} parameter, remains consistent across the entire frequency range of operation for the wide band. The design incorporates a Rohacell foam spacer between the MTM and the CPW antenna. This maintains a fixed distance and decreases electrical distraction between the two elements. During the fabrication process, ShieldIT super and flexible felt for the CPW antenna were manually cut. Fig. 7(a) depicts the front position of the fabricated wearable textile antenna. The 5 × 5 array's MTM X-shaped pattern is located on the back side of the CPW antenna. A computer numerical control (CNC) machine engraves the MTM. We attach the feedline and ground of the CPW antenna to the SMA port using silver epoxy. Fig. 7(b) presents the experimental setup for reflection coefficient measurement using a vector network analyzer (VNA) from Agilent Technologies model N5242A. The 5 × 5 cell arrays were selected for their superior bandwidth and gain performance relative to the 3 × 3 and 4 × 4 cell configurations, as depicted in Fig. 8.

The analysis of the proposed design is shown in Figs. 9 and 10. Even though the reflection coefficient exhibits slight alterations at certain frequencies and changes in resonance frequencies, as displayed in Fig. 9, the outputs between the simulated and measured coefficient values remain acceptable. More importantly, the impedance bandwidth ($S_{11} \leq -10$ dB)

(a) (b)

Fig. 7. CPW MTM antenna (a) fabricated antenna with MTM array and (b) experimental measurement setup.

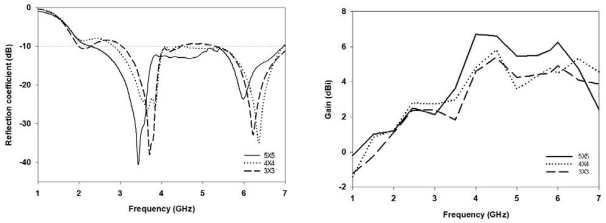

(a) (b)

Fig. 8. CPW and MTM antenna unit cell arrays comparison of (a) reflection coefficient and (b) gain.

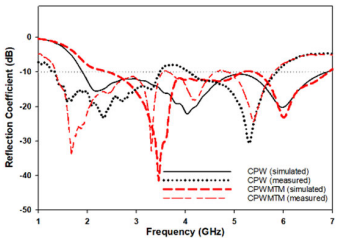

Fig. 9. Comparison of reflection coefficient for simulated and measured CPW and CPWMTM antennas.

covers the wideband frequency region needed for the objective of this design.

The study's findings highlight that the CPWMTM antenna successfully operates across a broad frequency range, spanning from 1.6 to 5.9 GHz. This wide bandwidth contrasts slightly with simulation results but generally aligns, suggesting a 26% increase in impedance bandwidth in testing. Fig. 9 details the reflection coefficient measurements, comparing the CPW antenna's performance with and without MTM integration. Without MTM, the CPW antenna achieves dual-band operation, covering 1.4–3.5 and 4.2–5.8 GHz. With MTM integration, however, the antenna achieves a continuous wideband response by effectively eliminating this notch (3.5–4.2 GHz). The integration of MTMs highlights the CPWMTM antenna's reliable spectrum performance. There is a noted slight difference between the measurement and simulation results, primarily due to a 50-Ω impedance mismatch across various frequency bands [41], material property variations [42], feed structure mismatches [43], fabrication tolerances [44], environmental influences, and simulation approximations [24], [45]. Additionally, manually cutting the antenna and unit cells may lead to a cumulative shift in the operating frequency.

Furthermore, comparing the antennas with and without the MTM, it is evident that the MTM arrays have the potential to enhance both the current intensity and gain [19]. Fig. 10 illustrates that integrating an MTM structure with the antenna

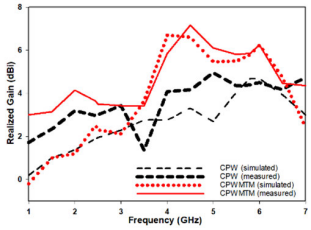

Fig. 10. Comparison of simulated and measured gain of CPW and CPWMTM antennas.

increased simulated gain from 4.6 to 6.7 dBi and spiked measured gain from 4.9 to 7.2 dBi.

Consequently, it can be concluded that the MTM construction significantly improves the antenna's gain. A significant rise in a certain direction corresponds to a greater concentration of power. In the context of wearable applications, employing an antenna with greater gain will increase directivity [46]. The results reveal that the proposed CPWMTM overcomes the decrease in gain at 3.5-GHz frequency due to the notch that appears while measuring the CPW antenna. The MTM acts as a reflector at 3.30–4.25 and 2.9–4.3 GHz due to ENG MTM characteristics [10].

Then, Fig. 11 displays the simulated radiation patterns in the *XZ* planes (phi = 0°) and *YZ* planes (phi = 90°), both with and without MTM. The measured radiation pattern utilizes a far-field anechoic chamber named the Atenlab OTA. This controller includes an antenna positioner controller, a VNA, and a tracking computer equipped with software for drawing radiation patterns. In the antenna with an MTM structure, the radiation increases in the forward direction, accompanied by reduced back lobes, compared to the antenna without MTM. Moreover, the MTM structure does not alter the broadside direction of the antenna at lower frequencies.

Afterward, Fig. 12 illustrates the surface current distribution of a CPW antenna with and without an MTM construction. The primary electric current circulates through the feedline and the parallel ground of a CPW antenna. Implementing the MTM structure enhances the visibility of current flow toward the far edge of the radiating patch. The current extends from the feedline to the radiating patch. At lower frequencies, the CSRR in a CPW antenna concentrates the surface current at the outer ring, whereas at higher frequencies, it concentrates the current at the inner ring. The equivalent circuit of CSRR that implements the inner and outer rings was explained in [47].

The MTM enhances the observable visibility of the CSRR surface current at the radiating patch. As displayed in Fig. 12(a) and (c), the current concentration reaches its maximum at 3.5 GHz and its minimum at 5.8 GHz, respectively. The induced current at these frequencies is observed to circulate in a ring loop, confirming the presence of magnetic resonance at all three frequencies [48]. The phenomenon of magnetic resonance amplifies the energy of EM waves. Thus, acquiring improved signal strength and coverage is of the utmost importance. The fabricated antenna's bending analysis was conducted using cylinder foam with diameters of 40 and 60 mm, as depicted in Fig. 13. The results demonstrate that both conditions fully cover the entire 5-GHz bandwidth,

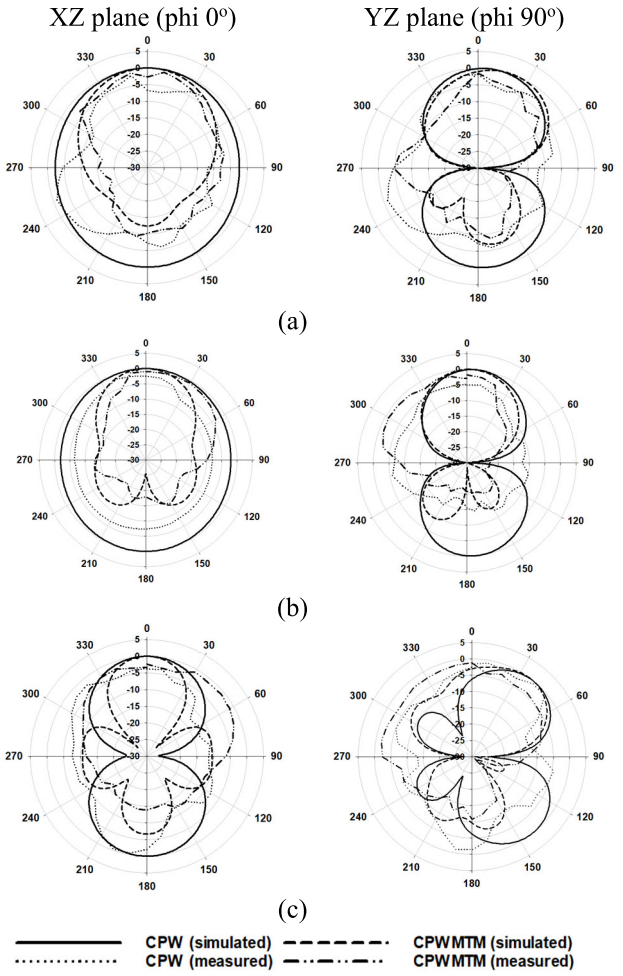

Fig. 11. Comparison of simulation and measurement 2-D radiation patterns of the antenna with and without MTM at frequencies of (a) 3.5, (b) 4.5, and (c) 5.8 GHz at phi = 0° and 90°.

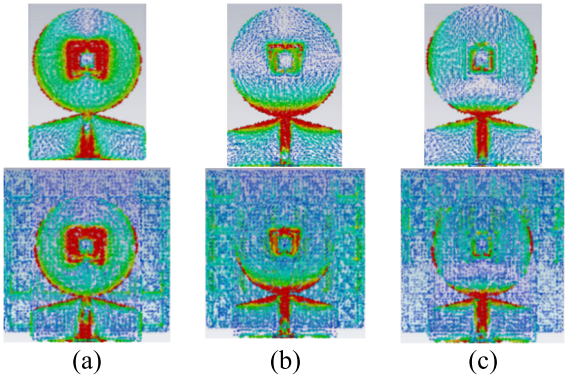

Fig. 12. Surface current distribution for CPW antenna with and without MTM structure at frequencies of (a) 3.5, (b) 4.5, and (c) 5.8 GHz.

confirming their suitability for practical applications in wearable MWI.

IV. MWI Application Validation

This study employed a cylindrical breast phantom consisting of three layers to better understand how antennas function close to human skin. The breast phantom maintains the same layers. However, it replaces the skin layer with a glass cover layer. Fig. 14(a) describes the experimental setup. The object consists of a cylindrical tube with a diameter of 90 mm and a

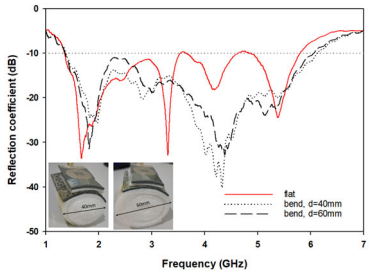

Fig. 13. Measurement result for flat and bending conditions of CPWMTM antenna.

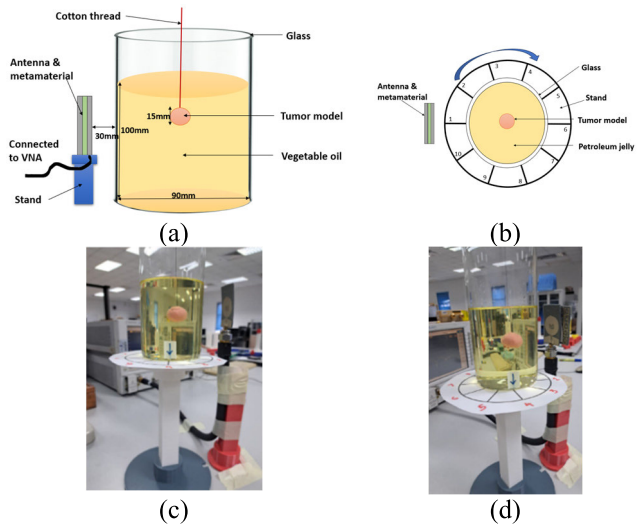

Fig. 14. CPW and MTM fabric antenna. (a) Experimental setup, (b) rotation of cylinder glass to obtain ten sets of readings, (c) CPW antenna with tumor model, and (d) CPW and MTM with tumor model.

height of 180 mm. Vegetable oil fills the cylinder to a height of 100 mm. A 2-mm-thick glass tube replaces the circular glass tube, mimicking the skin's thickness. The glass is a lossless material and is utilized to imitate the thinness of the skin, which measures just 2 mm, with minimum loss of effectiveness [49]. Another researcher used glass to mimic the skin, as suggested in [50] and [51].

The vegetable oil was selected as the dielectric filler for safety and cost considerations since it has been previously utilized in [16], [52], and [53]. To experimentally verify the simulation model, we monitored the reflection coefficient for each mentioned configuration using a VNA. This was conducted with a phantom with oil, with and without a tumor in the phantom. The antennas were placed 30 mm from the container and connected to the VNA using coaxial wires. The scattering material utilized to simulate tumors, comprised of 12 g of plasticine, exhibits a relative permittivity of 5–5.5 when subjected to a frequency of 1–10 GHz. Other than that, plasticine was also used by [54] to depict tumors of the breast phantom.

It signifies that the antenna is resistant to changes in tissue characteristics and continues functioning in the wideband frequency range. Therefore, it was determined that glass, vegetable oil, and plasticine materials would be utilized to create a proof-of-concept model in image reconstruction. In the measurement, one antenna emits signals and receives them in a monostatic setup, capturing both reflected and transmitted

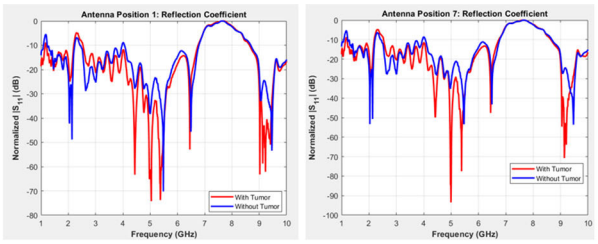

Fig. 15. Variations of the reflection parameter of the fabric MWI sensor.

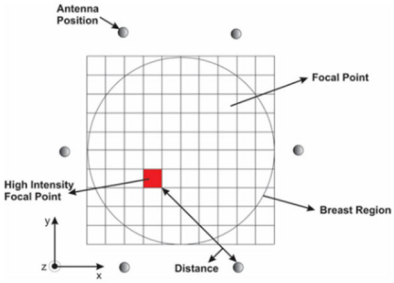

Fig. 16. Interpretation of the monostatic approach [57].

waves. To realize the precise position of the tumor, the phantom is systematically rotated along its axis in angular increments of 36°, as displayed in Fig. 14(b). The antenna horizontally scans the model in the *XY* plane at ten distinct points. The antenna measures a complete set of 1001 scattering parameters spanning the specified wideband frequency range of 1–10 GHz during each scan. The extracted data of reflection parameters from the sensor are shown in Fig. 15. This range covers both tumor and nontumor situations. The shift particularly between 3 and 6 GHz demonstrates that the presence of a tumor significantly alters the backscattered response across the frequency bands. This shift indicates enhanced dielectric contrast sensitivity, confirming that the sensor improves localized field confinement and backscatter detection [55]. The data obtained by VNA will be processed using monostatic radar-based DAS-beamforming or confocal MWI technique programmed in MATLAB. These signals are converted into the time domain using the inverse fast Fourier transform (IFFT) to remove artifacts and backscatter for better spatial resolution. This confocal MWI technique is highly regarded and extensively used for reconstructing lesion images using equations in the flowcharts [26].

The monostatic DAS-beamforming MWI technique segments the breast region into a narrow grid of focus points, as illustrated in Fig. 16. The distance between antenna locations and pixel points is computed and transformed into a propagation time delay using the average wave speed. The intensity corresponding to the pixel locations is assessed by summing and squaring the delayed copies of all received signals to generate a picture. Throughout the focusing process, the center of focus shifts around the breast phantom area [56]. At time $t_{XY}(xi,\ yj)$, the intensity values for each processed signal $P_{XY}(t)$ are generated by computing the values for each antenna location $(X,\ Y)$.

The pixel intensity I_{XY} of the reconstructed image can be articulated as (1), where n is the total number of antenna positions in a row, m is the total number of antenna positions

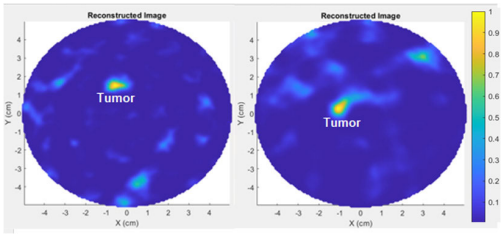

Fig. 17. Reconstructed image of breast tumor using DAS beamforming approaches (a) without MTM and (b) with MTM.

in a column, and $I\ (xi,\ yj)$ is the intensity value at $(xi,\ yj)$ pixel point [26], [57]. The processed signal $P_{XY}(t)$ is derived by subtracting the averaged signals from each breast phantom signal, reducing clutter caused by environmental, equipment, and antenna reflections. The round-trip distance to pixel t_{XY} is calculated using (2), considering the speed of light (c) and the medium's permittivity (εr). Equation (3) determines antenna distance D_{XY} to pixel $(xi,\ yj)$. In this context, h denotes the antenna's height from the skin along the Z-axis, indicating Z coordinates; xi and yj signify the coordinates of the pixel point, while X and Y represent the locations of the antenna sensor. The round-trip distance is doubled due to the monostatic radar method used [56]

$$I\ (xi,\ yj) = \left[\sum_{X=1}^{n}\sum_{Y=1}^{m} P_{XY}\ (t_{XY}\ (xi,\ y\ \ j))\right]^4 \tag{1}$$

$$t_{XY}\ (xi.y\ \ j) = \frac{D_{XY}\ (Xi,\ Y\ \ j)}{c/\sqrt{\varepsilon}\mathrm{r}} \tag{2}$$

$$D_{XY}\ (Xi,\ Y\ \ j) = 2\sqrt{(X-xi)^2 + (Y-Yi)^2 + h^2}. \tag{3}$$

According to this formula, the MATLAB code reconstructs the image. Incorporating MTM appears to reduce the shift of the antenna's image from its actual position, suggesting that MTM enhances the accuracy and control of the antenna's image. The imaging results for the proposed system, which uses a CPW antenna, are displayed in Fig. 17(a) and (b), with and without MTM, respectively. The tumor center is identified at (−0.5, 1.5) without MTM and located at (−0.9, 0.4) with MTM. Applying the Euclidean distance formula [58] reveals that employing MTM reduces the distance between these points from 1.61 to 1.04.

Finally, Table III compares the proposed sensor with related works. Tumor imaging using flexible multisensor systems was demonstrated in [19] and [22], while single-sensor studies [12], [17], [18], and [21] did not provide imaging results. Danjuma et al. [16] use a single sensor, but it is from a rigid profile. Another single rigid sensor by [15] achieved imaging, which required 36 sensor positions. Rigid MTM-based sensors reported by [10] and [11] demonstrated tumor imaging using multiple antenna configurations, ten sensing positions with two antennas along the x- and y-axes, and a dual-antenna system requiring 15° rotational steps around the phantom, respectively. Meanwhile, designs incorporating AMC structures, such as those by [13], involved complex geometries despite offering bistatic imaging capability. The sensors were relatively bulky, with dimensions of approximately 100 × 100 × 33 mm^3,

TABLE III
COMPARISON OF THE PROPOSED SENSOR AND PREVIOUS RELATED WORK

Year, Researcher	BW (GHz)	Gain range (dBi)	Physical length (mm x mm x mm)	Flexible material	MTM inclusion	Tumor model	Measured tumor image	Num. of sensors	Num. of locations	Sensor set up	Design complexity
2024, [10]	3.5 to 13	2 to 6	20 x 20 x 10.15	No	Yes	Yes	Yes	2	20	Bistatic	Low
2024, [12]	2 to 3	0.5 to 4.5	94 x 77 x 11	No	Yes	No	No	1	1	Monostatic	Low
2024, [13]	2 to 14	-10 to 11.7	35.6 x 35.6 x 6.04	No	Yes	No.	No	4	1	Multistatic	High
2023, [14]	2.3 to 2.9	NR	100 x 100 x 33.3	No	Yes	Yes	Yes	2	1	Bistatic	Medium
2023, [17]	2.5 to 9	-2 to 10	50 x 50 x 2	Yes	No	Yes	No	1 & 2	1	Monostatic & Bistatic	Low
2023, [18]	1.8 to 8	3 to 6	33.5 × 33.5 x 2	Yes	No	Yes	No	1 & 2	1	Monostatic & Bistatic	Low
2022, [11]	0.5 to 2	4.8 dB (average)	24.7 x 29.7 x 2.54	No	Yes	Yes	Yes	2	24	Multistatic	Low
2022, [19]	2.4 to 3.3 & 4 to 15	2 to 7.56	61 x 80 x 3	Yes	Yes	Yes	Yes	2 & 4	36	Bistatic & Multistatic	High
2022, [22]	3.9–19.0	NR	38.3 x 27.1 x 0.8	Yes	No	Yes	Yes	8	1	Multistatic	Low
2021, [15]	4.3 to 12.6	2 to 6 dB	20 x 15 x 5.64	No	No	Yes	Yes	1	36	Monostatic	Low
2021, [20]	6.5 to 35	2.5 to 8.85	10 x 15 x 2.2	Yes	Yes	No	No	12	1	Multistatic	High
2020, [16]	3 to 10	2.5 to 4.7	33 x 15 x 0.8	No	No	Yes	Yes	1	NR	Monostatic	Low
2019, [21]	1.106 to 1.110	NR	125 x 51 x 1.52	Yes	No	Yes	No	1	5	Monostatic	Low
Proposed work	2.4 to 6.9	2.2 to 6.7	53 x 58 x 9.51	Yes	Yes	Yes	Yes	1	10	Monostatic	Low

*NR: Not reported

and exhibited narrow operational bandwidths [14]. Similarly, MTM-based flexible sensors presented by [19] utilized two or four antennas with 10° mechanical rotations to capture scattered signals, while Alhawari et al. [20] employed 12 fixed antennas positioned around the phantom.

In contrast, the proposed work introduces a fully textile-based, MTM-integrated antenna optimized for microwave breast imaging with a single sensing element. By incorporating CSRR and X-shaped MTM structures, the design achieves wide bandwidth, high efficiency, and compactness. Unlike conventional multiantenna or rigid systems that require extensive scanning, the proposed sensor achieves effective imaging with only ten azimuthal rotations, demonstrating a low-complexity and efficient single-sensor solution.

This single, fabric-based antenna is more cost-effective and practical for wearable applications than other systems that need an external power supply or complicated multistatic configurations. The antenna's stable gain of 5 dBi and 88% radiation efficiency across a 2.4–6.9-GHz bandwidth further demonstrates its suitability for MWI in realistic tumor models. It significantly simplifies breast tumor imaging, reducing setup complexity while achieving promising imaging results. Accordingly, this research highlights the potential of fabric-integrated MTM antennas for advanced, noninvasive MWI applications, supporting portable, user-friendly diagnostic tools suitable for real-world clinical and wearable environments. Furthermore, the influence of material consistency on different bending and crumpling effects should be considered. The safety criteria regarding the distance between the body, the duration of use, and power consumption are also intriguing to explore in the future.

V. CONCLUSION

In conclusion, the proposed antenna demonstrates marked advancements in MWI for tumor detection. Integrating MTMs enhances the reflection coefficient and gain, resulting in a broader bandwidth and improved stability. The antenna effectively detects a 15-mm tumor with minimal image displacement by leveraging an advanced MTM structure and DAS algorithm. Note that the antenna operates in a broad frequency range, ranging from 2.4 to 6.9 GHz in simulation and from 1.6 to 5.9 GHz in measurement. The proposed sensor achieves maximum gains from 6.7 dBi (simulated) to 7.2 dBi (measured), demonstrating high performance and reliability. Furthermore, these findings validate the feasibility of adaptable, MTM-enhanced single-antenna systems for tumor identification, providing promising gain and bandwidth. Nevertheless, this design establishes itself as a competent solution for wearable medical imaging applications, and it has the potential to expand to wireless on-body communications.

REFERENCES

[1] World Health Oganization. (2024). *Breast Cancer*. Accessed: Aug. 15, 2024. [Online]. Available: https://www.who.int/news-room/fact-sheets/detail/breast-cancer

[2] C. Das, M. Z. Chowdhury, and Y. M. Jang, "A novel miniaturized mmWave antenna sensor for breast tumor detection and 5G communication," *IEEE Access*, vol. 10, pp. 114856–114868, 2022, doi: 10.1109/ACCESS.2022.3216858.

[3] A. A. Abdul Halim et al., "Existing and emerging breast cancer detection technologies and its challenges: A review," *Appl. Sci.*, vol. 11, no. 22, p. 10753, Nov. 2021, doi: 10.3390/app112210753.

[4] H. M. E. Misilmani, T. Naous, S. K. A. Khatib, and K. Y. Kabalan, "A survey on antenna designs for breast cancer detection using microwave imaging," *IEEE Access*, vol. 8, pp. 102570–102594, 2020, doi: 10.1109/ACCESS.2020.2999053.

[5] M. Z. Mahmud, M. T. Islam, N. Misran, S. Kibria, and M. Samsuzzaman, "Microwave imaging for breast tumor detection using uniplanar AMC based CPW-fed microstrip antenna," *IEEE Access*, vol. 6, pp. 44763–44775, 2018, doi: 10.1109/ACCESS.2018.2859434.

[6] A. S. M. Alqadami, N. Nguyen-Trong, B. Mohammed, A. E. Stancombe, M. T. Heitzmann, and A. Abbosh, "Compact unidirectional conformal antenna based on flexible high-permittivity custom-made substrate for wearable wideband electromagnetic head imaging system," *IEEE Trans. Antennas Propag.*, vol. 68, no. 1, pp. 183–194, Jan. 2020, doi: 10.1109/TAP.2019.2938849.

[7] Z. Gong, Y. Chen, X. Lin, K. Wu, and M. J. Cree, "Generic wideband phantom design methodology for microwave medical applications," *IEEE Antennas Wireless Propag. Lett.*, vol. 20, no. 8, pp. 1488–1492, Aug. 2021, doi: 10.1109/LAWP.2021.3088449.

[8] A. Naghibi and A. R. Attari, "Near-field radar-based microwave imaging for breast cancer detection: A study on resolution and image quality," *IEEE Trans. Antennas Propag.*, vol. 69, no. 3, pp. 1670–1680, Mar. 2021, doi: 10.1109/TAP.2020.3016407.

[9] M. K. D. Menon and J. Rodrigues, "Efficient ultra wideband radar based non invasive early breast cancer detection," *IEEE Access*, vol. 11, pp. 84214–84227, 2023, doi: 10.1109/ACCESS.2023.3303333.

[10] F.-E. Zerrad, M. Taouzari, E. Almajali, M. Karaaslan, J. E. Aoufi, and A. Hussain, "An improved breast cancer biosensing system using a slotted patch antenna with a metamaterial surface," *IEEE Sensors J.*, vol. 25, no. 1, pp. 634–646, Jan. 2025, doi: 10.1109/JSEN.2024.3476691.

[11] N. Ghavami et al., "The use of metasurfaces to enhance microwave imaging: Experimental validation for tomographic and radar-based algorithms," *IEEE Open J. Antennas Propag.*, vol. 3, pp. 89–100, 2022, doi: 10.1109/OJAP.2021.3135146.

[12] K. Youssef, M. Abo-Zahhad, H. Kanaya, and A. H. Abd El-Malek, "A unified approach for breast cancer discrimination using metasurface-based microwave technology," *Discover Appl. Sci.*, vol. 6, no. 8, p. 395, Jul. 2024, doi: 10.1007/s42452-024-06005-x.

[13] M. N. Hamza, M. T. Islam, and S. Koziel, "Advanced sensor for non-invasive breast cancer and brain cancer diagnosis using antenna array with metamaterial-based AMC," *Eng. Sci. Technol., Int. J.*, vol. 56, Aug. 2024, Art. no. 101779, doi: 10.1016/j.jestch.2024.101779.

[14] D. Brizi, M. Conte, and A. Monorchio, "A performance-enhanced antenna for microwave biomedical applications by using metasurfaces," *IEEE Trans. Antennas Propag.*, vol. 71, no. 4, pp. 3314–3323, Apr. 2023, doi: 10.1109/TAP.2023.3242414.

[15] G. Kaur and A. Kaur, "Monostatic radar-based microwave imaging of breast tumor detection using a compact cubical dielectric resonator antenna," *Microw. Opt. Technol. Lett.*, vol. 63, no. 1, pp. 196–204, Jan. 2021, doi: 10.1002/mop.32557.

[16] I. M. Danjuma, M. O. Akinsolu, C. H. See, R. A. Abd-Alhameed, and B. Liu, "Design and optimization of a slotted monopole antenna for ultra-wide band body centric imaging applications," *IEEE J. Electromagn., RF Microw. Med. Biol.*, vol. 4, no. 2, pp. 140–147, Jun. 2020, doi: 10.1109/JERM.2020.2984910.

[17] D. M. Elsheakh, S. A. Alsherif, and A. R. Eldamak, "Textile monopole sensors for breast cancer detection," *Telecommun. Syst.*, vol. 82, no. 3, pp. 363–379, Mar. 2023, doi: 10.1007/s11235-023-00990-x.

[18] D. N. Elsheakh, Y. K. Elgendy, M. E. Elsayed, and A. R. Eldamak, "Circularly polarized textile sensors for microwave-based smart bra monitoring system," *Micromachines*, vol. 14, no. 3, p. 586, Feb. 2023, doi: 10.3390/mi14030586.

[19] K. Hossain, T. Sabapathy, M. Jusoh, S.-H. Lee, K. S. A. Rahman, and M. R. Kamarudin, "Negative index metamaterial-based frequency-reconfigurable textile CPW antenna for microwave imaging of breast cancer," *Sensors*, vol. 22, no. 4, p. 1626, Feb. 2022, doi: 10.3390/s22041626.

[20] A. R. H. Alhawari, A. H. M. Almawgani, A. T. Hindi, H. Alghamdi, and T. Saeidi, "Metamaterial-based wearable flexible elliptical UWB antenna for WBAN and breast imaging applications," *AIP Adv.*, vol. 11, no. 1, p. 2021, Jan. 2021, doi: 10.1063/5.0037232.

[21] M. A. Aldhaeebi, T. S. Almoneef, H. Attia, and O. M. Ramahi, "Near-field microwave loop array sensor for breast tumor detection," *IEEE Sensors J.*, vol. 19, no. 24, pp. 11867–11872, Dec. 2019, doi: 10.1109/JSEN.2019.2936993.

[22] H. Li, H. Zhang, Y. Kong, and C. Zhou, "Flexible dual-polarized UWB antenna sensors for breast tumor detection," *IEEE Sensors J.*, vol. 22, no. 13, pp. 13648–13658, Jul. 2022, doi: 10.1109/JSEN.2022.3180356.

[23] M. Abdolrazzaghi and M. Daneshmand, "A 4 GHz near-field monitoring planar oscillator sensor," in *IEEE MTT-S Int. Microw. Symp. Dig.*, Jul. 2018, pp. 1–3, doi: 10.1109/IMWS-AMP.2018.8457169.

[24] N. Hosseini, S. S. Olokede, and M. Daneshmand, "A novel miniaturized asymmetric CPW split ring resonator with extended field distribution pattern for sensing applications," *Sens. Actuators A, Phys.*, vol. 304, Apr. 2020, Art. no. 111769, doi: 10.1016/j.sna.2019.111769.

[25] N. Hosseini and M. Baghelani, "Selective real-time non-contact multi-variable water-alcohol-sugar concentration analysis during fermentation process using microwave split-ring resonator based sensor," *Sens. Actuators A, Phys.*, vol. 325, Jul. 2021, Art. no. 112695, doi: 10.1016/j.sna.2021.112695.

[26] M. A. Jamlos et al., "Ultra-wideband confocal microwave imaging for brain tumor detection," *IOP Conf. Series: Mater. Sci. Eng.*, vol. 557, no. 1, Jun. 2019, Art. no. 012002, doi: 10.1088/1757-899x/557/1/012002.

[27] A. Mirbeik-Sabzevari, S. Li, E. Garay, H.-T. Nguyen, H. Wang, and N. Tavassolian, "Synthetic ultra-high-resolution millimeter-wave imaging for skin cancer detection," *IEEE Trans. Biomed. Eng.*, vol. 66, no. 1, pp. 61–71, Jan. 2019, doi: 10.1109/TBME.2018.2837102.

[28] A. H. Naghavi, H. R. Hassani, and D. Oloumi, "Investigation and analysis of EM pulse propagation inside human head for high-resolution UWB elliptical SAR imaging," *IEEE J. Electromagn., RF Microw. Med. Biol.*, vol. 6, no. 4, pp. 485–493, Dec. 2022, doi: 10.1109/JERM.2022.3182879.

[29] A. Mirbeik-Sabzevari, N. Tavassoian, and R. Ashinoff, "Ultra-high-resolution millimeter-wave imaging: A new promising skin cancer imaging modality," in *Proc. IEEE Biomed. Circuits Syst. Conf. (BioCAS)*, Oct. 2018, pp. 1–4, doi: 10.1109/BIOCAS.2018.8584772.

[30] N. AlSawaftah, S. El-Abed, S. Dhou, and A. Zakaria, "Microwave imaging for early breast cancer detection: Current state, challenges, and future directions," *J. Imag.*, vol. 8, no. 5, p. 123, Apr. 2022, doi: 10.3390/jimaging8050123.

[31] LessEMF. (2011). *Shieldit Super Fabric*. Accessed: Dec. 12, 2022. [Online]. Available: https://lessemf.com/product/shieldit-super-fabric/

[32] U. Ali, A. Basir, M. Zada, S. Ullah, B. Kamal, and H. Yoo, "Performance improvement of a dual-band textile antenna for on-body through artificial magnetic conductor," *IEEE Access*, vol. 11, pp. 72316–72331, Jul. 2023, doi: 10.1109/ACCESS.2023.3294412.

[33] N. Gupta, J. Saxena, K. S. Bhatia, and R. Kumar, "A compact CPW-fed planar stacked circle patch antenna for wideband applications," *Wireless Pers. Commun.*, vol. 116, no. 4, pp. 3247–3260, Feb. 2021, doi: 10.1007/s11277-020-07847-5.

[34] O. Fiser et al., "UWB bowtie antenna for medical microwave imaging applications," *IEEE Trans. Antennas Propag.*, vol. 70, no. 7, pp. 5357–5372, Jul. 2022, doi: 10.1109/TAP.2022.3161355.

[35] M. Alibakhshikenari et al., "Metamaterial-inspired antenna array for application in microwave breast imaging systems for tumor detection," *IEEE Access*, vol. 8, pp. 174667–174678, 2020, doi: 10.1109/ACCESS.2020.3025672.

[36] M. Alibakhshikenari et al., "A comprehensive survey of 'metamaterial transmission-line based antennas: Design, challenges, and applications,'" *IEEE Access*, vol. 8, pp. 144778–144808, 2020, doi: 10.1109/ACCESS.2020.3013698.

[37] C. Milias et al., "Metamaterial-inspired antennas: A review of the state of the art and future design challenges," *IEEE Access*, vol. 9, pp. 89846–89865, 2021, doi: 10.1109/ACCESS.2021.3091479.

[38] M. Asif et al., "Design of a dual band SNG metamaterial based antenna for LTE 46/WLAN and Ka-band applications," *IEEE Access*, vol. 9, pp. 71553–71562, 2021, doi: 10.1109/ACCESS.2021.3077844.

[39] M. Moniruzzaman, M. T. Islam, M. R. Islam, N. Misran, and M. Samsuzzaman, "Coupled ring split ring resonator (CR-SRR) based epsilon negative metamaterial for multiband wireless communications with high effective medium ratio," *Results Phys.*, vol. 18, Sep. 2020, Art. no. 103248, doi: 10.1016/j.rinp.2020.103248.

[40] M. T. Islam, M. Samsuzzaman, S. Kibria, N. Misran, and M. T. Islam, "Metasurface loaded high gain antenna based microwave imaging using iteratively corrected delay multiply and sum algorithm," *Sci. Rep.*, vol. 9, no. 1, pp. 1–14, Nov. 2019, doi: 10.1038/s41598-019-53857-0.

[41] N. K. Sahu and S. K. Mishra, "Compact dual-band dual-polarized monopole antennas using via-free metasurfaces for off-body communications," *IEEE Antennas Wireless Propag. Lett.*, vol. 21, no. 7, pp. 1358–1362, Jul. 2022, doi: 10.1109/LAWP.2022.3167849.

[42] U. Ali, S. Ullah, B. Kamal, L. Matekovits, and A. Altaf, "Design, analysis and applications of wearable antennas: A review," *IEEE Access*, vol. 11, pp. 14458–14486, 2023, doi: 10.1109/ACCESS.2023.3243292.

[43] V. Marterer, M. Radouchová, R. Soukup, S. Hipp, and T. Blecha, "Wearable textile antennas: Investigation on material variants, fabrication methods, design and application," *Fashion Textiles*, vol. 11, no. 1, pp. 1–28, Feb. 2024, doi: 10.1186/s40691-023-00369-1.

[44] X. Lin, Y. Chen, Z. Gong, B.-C. Seet, L. Huang, and Y. Lu, "Ultrawideband textile antenna for wearable microwave medical imaging applications," *IEEE Trans. Antennas Propag.*, vol. 68, no. 6, pp. 4238–4249, Jun. 2020, doi: 10.1109/TAP.2020.2970072.

[45] N. Hosseini, M. Baghelani, and M. Daneshmand, "Selective volume fraction sensing using resonant- based microwave sensor and its harmonics," *IEEE Trans. Microw. Theory Techn.*, vol. 68, no. 9, pp. 3958–3968, Sep. 2020, doi: 10.1109/TMTT.2020.2990139.

[46] C. A. Balanis, *Antenna Theory: Analysis and Design*. Hoboken, NJ, USA: Wiley, 2005.

[47] I. S. A. Razak et al., "A fabric-based double rectangular complementary split ring resonator for wideband applications," *Prog. Electromagn. Res. C*, vol. 157, pp. 147–158, 2025, doi: 10.2528/PIERC25031003.

[48] D. Negi, R. Khanna, and J. Kaur, "Design and performance analysis of a conformal CPW fed wideband antenna with mu-negative metamaterial for wearable applications," *Int. J. Microw. Wireless Technol.*, vol. 11, no. 8, pp. 806–820, Oct. 2019, doi: 10.1017/s1759078719000497.

[49] S. Alshehri, A. Jantan, R. S. A. Raja Abdullah, R. Mahmud, S. Khatun, and Z. Awang, "A UWB imaging system to detect early breast cancer in heterogeneous breast phantom," in *Proc. Int. Conf. Electr., Control Comput. Eng. (InECCE)*, Jun. 2011, pp. 238–242, doi: 10.1109/INECCE.2011.5953883.

[50] B. S. Bari et al., "Ultra wide band (UWB) based early breast cancer detection using artificial intelligence," in *Proc. 5th Int. Conf. Elect., Control Comput. Eng.*, Jan. 2020, pp. 505–515, doi: 10.1007/978-981-15-2317-5_43.

[51] T. Reimer and S. Pistorius, "An optimization-based approach to radar image reconstruction in breast microwave sensing," *Sensors*, vol. 21, no. 24, pp. 1–15, Dec. 2021, doi: 10.3390/s21248172.

[52] D. Oloumi, R. S. C. Winter, A. Kordzadeh, P. Boulanger, and K. Rambabu, "Microwave imaging of breast tumor using time-domain UWB circular-SAR technique," *IEEE Trans. Med. Imag.*, vol. 39, no. 4, pp. 934–943, Apr. 2020, doi: 10.1109/TMI.2019.2937762.

[53] A. F. Mirza et al., "An active microwave sensor for near field imaging," *IEEE Sensors J.*, vol. 17, no. 9, pp. 2749–2757, May 2017, doi: 10.1109/JSEN.2017.2673961.

[54] R. Rasappan, S. K. K. Mohd, N. S. N. Anwar, and M. Z. Abdullah, "Three-dimensional microwave breast cancer detection system based on bi-conical UWB antenna array," in *Proc. Ser. ACM Int. Conf.*, 2017, pp. 131–137, doi: 10.1145/3132300.3132306.

[55] M. K. Sharma et al., "Experimental investigation of the breast phantom for tumor detection using ultra-wide band–MIMO antenna sensor (UMAS) probe," *IEEE Sensors J.*, vol. 20, no. 12, pp. 6745–6752, Jun. 2020, doi: 10.1109/JSEN.2020.2977147.

[56] I. Amdaouch et al., "A novel approach of a low-cost UWB microwave imaging system with high resolution based on SAR and a new fast reconstruction algorithm for early-stage breast cancer detection," *J. Imag.*, vol. 8, no. 10, p. 264, Sep. 2022, doi: 10.3390/jimaging8100264.

[57] S. M. Salvador and G. Vecchi, "Experimental tests of microwave breast cancer detection on phantoms," *IEEE Trans. Antennas Propag.*, vol. 57, no. 6, pp. 1705–1712, Jun. 2009, doi: 10.1109/TAP.2009.2019901.

[58] M. Greenacre and R. Primicerio, *Measures of Distance Between Samples: Euclidean*, Multivar. Anal. Ecol. Data, 2013, pp. 47–59. [Online]. Available: http://www.pubmedcentral.nih.gov/articlerender.fcgi?artid=3018372&tool=pmcentrez&rendertype=abstract

Intan Shafinaz Abd. Razak received the B.Eng. degree in electrical engineering and technical and vocational education from Kolej Universiti Teknologi Tun Hussein Onn (KUiTTHO), Johor, Malaysia, in 2004, the M.Ed. degree from Universiti Teknologi Tun Hussein Onn (UTHM), Johor, in 2006, and the M.Eng. degree in electronic engineering from Universiti Teknikal Malaysia Melaka (UTeM), Durian Tunggal, Malaysia, in 2016, where she is currently pursuing the Ph.D. degree.

She joined Politeknik Tuanku Sultanah Bahiyah, Kedah, Malaysia, as a Lecturer, in 2006.

Ahmed Jamal Abdullah Al-Gburi (Senior Member, IEEE) received the M.Eng. and Ph.D. degrees in electronics and computer engineering telecommunication systems from Universiti Teknikal Malaysia Melaka (UTeM), Durian Tunggal, Malaysia, in 2017 and 2021, respectively.

He is currently a Senior Lecturer with the Faculty of Electronic and Computer Engineering Technology, UTeM.

Maizatul Alice Meor Said received the B.Eng. degree in electronics engineering telecommunication from the University of Surrey, Guildford, U.K., in 2006, and the Master of Engineering degree in telecommunications from the University of Wollongong, Wollongong, NSW, Australia, in 2009. She is currently pursuing the Ph.D. degree with Universiti Teknikal Malaysia Melaka (UTeM), Durian Tunggal, Malaysia.

Her research areas include RF energy harvesting, resonators, amplifiers, antennas, and microwave sensors.

Syah Alam (Member, IEEE) was born in Jakarta, Indonesia. He received the Bachelor of Education (S.Pd.) degree in electrical engineering from the Universitas Pendidikan Indonesia (UPI), Bandung, Indonesia, in 2010, the M.Eng (M.T.) degree in telecommunication engineering from the Graduate Program of Electrical Engineering, Universitas Trisakti, West Jakarta, Indonesia, in 2012, and the Ph.D. degree in electronic engineering (RF and microwave) from the Universiti Teknikal Malaysia Melaka (UTeM), Durian Tunggal, Malaysia, in 2024.

In 2018, he joined the Department of Electrical Engineering, Universitas Trisakti, West Jakarta, Indonesia, as a Researcher and a Lecturer. His research interests include microstrip antennas and microwave sensors for various applications.

Zahriladha Zakaria (Senior Member, IEEE) received the B.Eng. and M.Eng. degrees in electrical and electronic engineering from Universiti Teknologi Malaysia (UTM), Johor Bahru, Malaysia, in 1998 and 2004, respectively, and the Ph.D. degree in electrical and electronic engineering from the Institute of Microwaves and Photonics (IMP), University of Leeds, Leeds, U.K., in 2010.

He is currently the Deputy Vice Chancellor (Research and Innovation) and a Professor at the Microwave Research Group (MRG), Faculty of Electronic and Computer Engineering.

This author profile is generated by Scopus

Alam, Syah

Universitas Trisakti, Jakarta, Indonesia • Scopus ID: 57191903622 • 0000-0002-0162-8364

Show all information

353	77	11
Citations by **266** documents	Documents	*h*-index

Set alert | Save to list | Edit profile | More

Beta

Documents (77) | Impact | Cited by (266) | Preprints (1) | Co-authors (130) | Topics (15) | Awarded grants (0)

You can view, sort, and filter all of the documents in search results format.

Export all | Save all to list | Sort by Date (newest)

Article

A Single-Port Microwave Sensor Based on Interdigital Capacitor and Electromagnetic Coupled Structure for Permittivity Detection of Vegetables Materials

0 Citations

Sari, F.K., Alam, S., Surjati, I., ... Zakaria, Z., Shairi, N.A.

Sensing and Imaging, 2026, 27(1), 7

Show abstract Full text Related documents

Article

Independent and asymmetric coupling structure for integrated dual-band bandpass filter with microwave microfluidic milk sensor

0 Citations

Firmansyah, T., Praptodiyono, S., Muttakin, I., ... Iqbal, M., Nugraha

AEU International Journal of Electronics and Communications, 2026, 206, 156186

Show abstract Full text Related documents

Article

Fabric-Based Metamaterial-Integrated CPW Antenna for Microwave Tumor Sensing

0 Citations

Abd Razak, I.S., Al-Gburi, A.J.A., Meor Said, M.A., Alam, S., Zakaria, Z.

IEEE Sensors Journal, 2026, 26(3), pp. 3944–3953

Show abstract Full text Related documents

Don't miss out on new publications by this author!

Set document alert

Article • Article in Press

High-Q H-Shaped Nested Split-Ring Resonator Sensor for Liquid Complex-Permittivity Characterization

0 Citations

Rahman, M.Z.A., Idris, M.I., Jemaludin, N.H., ... Alam, S., Zakaria, Z.

IEEE Sensors Journal, 2026

Show abstract Full text Related documents

Article

Application of LT Code with BCH Precode for Wireless Body Area Network

Sari, L., Alam, S., Mardian, R.D., Surjati, I.

Journal of Electrical and Electronics Engineering, 2025, 18(2), pp. 63–68

0 Citations

Show abstract Full text Related documents

Article

Multifunctional microwave-plasmonic microfluidic sensor utilizing gold nanoparticles embedded in multilayered ring resonator

Firmansyah, T., Alfanz, R., Denny, Y.R., ... Wibisono, G., Kondoh, J.

Sensors and Actuators A Physical, 2025, 385, 116275

0 Citations

Show abstract Full text Related documents

Article • *Open access*

SAR Distribution with Different Water Bolus Shapes for Hyperthermia Breast Cancer Treatment

Hassan, M.M., Lias, K., Buniyamin, N., ... Basri, H.M., Alam, S.

Journal of Advanced Research in Fluid Mechanics and Thermal Sciences, 2025, 128(1), pp. 32–47

1 Citations

Show abstract Full text Related documents

Article • *Open access*

A Broadband Half-Mode Substrate Integrated Waveguide Cavity Antenna with Triple Resonances

Astuti, D.W., Majid, H.A., Alam, S., Setyawan, A.

Progress in Electromagnetics Research C, 2025, 152, pp. 55–66

2 Citations

Show abstract Full text Related documents

Article • *Open access*

Broadband HMSIW antenna using a demi hexagonal ring slot for X-band application

Astuti, D.W., Muslim, M., Umaisaroh, U., ... Alam, S., Rahayu, Y.

3 Citations

Sinergi Indonesia, 2025, 29(1), pp. 73–82

Show abstract Full text Related documents

Article

A Fabric-Based Double Rectangular Complementary Split Ring Resonator for Wideband Applications

1
Citations

Abd. Razak, I.S., Zakaria, Z., Al-Gburi, A.J.A., ... Alam, S., Palandoken, M.

Progress in Electromagnetics Research C, 2025, 157, pp. 147–158

Show abstract Full text Related documents

Previous 1 2 3 4 5 ... 8 Next

Display 10 results

View all references

Document & citation trends

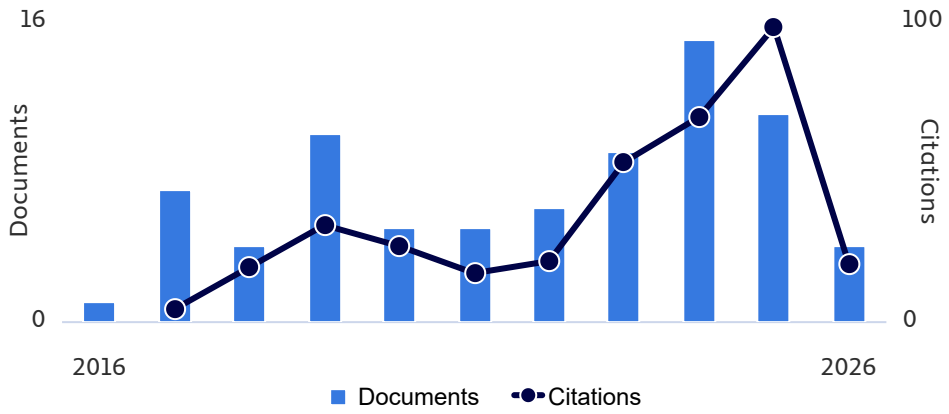

Citation overview Analyze author output

Author Position for 2015 - 2024

First author 49%

29 Documents | 5 Average citations | 0.689 FWCI

Last author 18%

Co-author 33%

Single author 0%

Show author position details

Back to top

About Scopus

What is Scopus

Content coverage

Scopus blog

Scopus API

Privacy matters

Language

日本語版を表示する

查看简体中文版本

查看繁體中文版本

Просмотр версии на русском языке

Customer Service

Help

Tutorials

Contact us